International Journal of Recent Advances in Multidisciplinary Topics
Volume 7, Issue 2, February 2026
www.ijramt.com | E-ISSN: 2582-7839 | RESAIM Publishing | www.resaim.com


# Variable Domain Fuzzy PID Driven Anti-Skid Control with Integrated Road Surface Recognition

Bingsen Liu[1*], Chengao Shi[1], Gang Chen[1], Wei Song[2], Yanmei Chen[2], Jin Ye[2], Liangmo Wang[1]
[1]School of Mechanical Engineering, Nanjing University of Science and Technology, Nanjing, China
[2]Electrical Department, NAVECO Ltd., Nanjing, China

***Abstract*: Traction control is a critical component in ensuring both vehicle performance and safety. Traditional traction control strategies, often based on fixed-parameter controllers, struggle to adapt to complex and variable road surface conditions. This is particularly evident on low-friction surfaces, where response delays or excessive intervention frequently occur. To address this, this paper proposes an integrated traction control method combining fuzzy road surface recognition with variable domain fuzzy PID control. A fuzzy inference system is constructed to achieve online identification of the optimal slip rate for the road surface. Based on this, a variable domain fuzzy PID controller with an adaptive scaling factor is designed. This controller dynamically adjusts its domain range according to the road surface recognition results and vehicle state, enabling precise and smooth regulation of drive torque. Joint simulations using CarSim and MATLAB demonstrate that the optimal slip rate recognition error is 5.3% on snow-covered surfaces and 4.7% on dry gravel surfaces. Compared to traditional PID and conventional fuzzy PID controllers, this strategy exhibits reduced overshoot, accelerates convergence of slip rates to optimal values across all wheels, and enhances vehicle stability during both acceleration and steady-state driving.**

***Keywords*: Traction Control, Road Surface Recognition, Fuzzy Control, Variable Domain Theory.**

## 1. Introduction

Electric vehicles offer significant advantages in drive response speed, precise torque control, and state monitoring [1]. Their drive anti-slip control has become a core technology for enhancing overall vehicle dynamics and active safety [2]. Leveraging the millisecond-level response characteristics of drive motors and precise wheel-end torque monitoring capabilities, electric vehicles can implement active torque vectoring control and real-time estimation of road surface friction coefficients. This effectively suppresses excessive drive wheel slip on low-friction surfaces or under extreme conditions, thereby improving acceleration stability [3].

Domestic and foreign scholars have conducted extensive research. Hiroshi Fujimoto's team [4] proposed a sensorless anti-slip control method based on back-EMF observers, addressing control challenges posed by traditional sensors at low speeds and during sensor failures. Alexander Busch et al. [5] introduced an adaptive model predictive anti-slip control strategy, overcoming the limitations of logic-based control on low-friction surfaces and the numerical instability issues of MPC at low speeds. Reza Jafari et al. [6] implemented torque vector control for four-wheel electric vehicles using the TD3 algorithm, achieving a dynamic equilibrium between energy optimization and anti-slip control within a model-free framework. Takumi Ueno et al. [7] designed a “wheel speed limiter” that resolves the conflict between longitudinal drive and lateral stability without enforcing slip rate locking. Nam T. Nguyen [8] proposed enhanced fuzzy model following control, significantly improving control accuracy under load variations and tire wear. Jin Liqiang's team [9] employed an UKF to identify peak road surface friction coefficients online and designed a robust anti-slip controller, effectively resolving drive force interruptions on uneven surfaces. Xiang Gao et al. [10] proposed an electromechanical coupling anti-slip strategy that combines road surface recognition with sliding mode control, achieving both precise anti-slip performance and vehicle energy efficiency. Bo Leng [11] employs dual observers for dynamics and kinematics to estimate vehicle speed and slip rate, utilizing sliding mode and PI control methods to design a saturation-resistant controller. Zhuoping Yu [12] derives the optimal reference slip rate based on non-affine parameter estimation theory and designs a state feedback control law using Lyapunov theory to achieve smooth switching between driver intent and optimal drive torque.

To address the issue of excessive controller response during wheel slip in electric vehicles on complex road surfaces, this paper proposes a traction control strategy integrating road surface recognition with variable domain fuzzy PID control. This approach achieves rapid and precise traction control responses under complex road conditions, enhancing the controller's robustness across diverse operating scenarios.

## 2. Vehicle Dynamics Modeling

### *A. Wheel Rotation Dynamics Model*

As shown in Figure 1, combined with wheel dynamics, it can be seen that:

$$I_\omega \dot{\omega}_{ij} = T_{d_{ij}} - F_{x_{ij}} R \tag{1}$$

*Corresponding author: 19164012062@163.com

Where,

$I_\omega$=Wheel rotational inertia

$\dot{\omega}_{ij}$=Angular acceleration of each wheel

$T_{d_{ij}}$=Drive torque of each wheel

$F_{x_{ij}}$=Ground tangential reaction force along the x-axis

From equation (1), the longitudinal force on each wheel is obtained as:

$$F_{x_{ij}} = \frac{T_{d_{ij}} - I_\omega \dot{\omega}_{ij}}{R} \tag{2}$$

During vehicle operation, longitudinal acceleration of the wheels causes axle load transfer between wheels. Therefore, the vertical wheel force is calculated as shown in Formula (3):

$$\begin{cases} F_{zL1} = mg\dfrac{b}{2L} - ma_x\dfrac{h_g}{2L} \\ F_{zR1} = mg\dfrac{b}{2L} - ma_x\dfrac{h_g}{2L} \\ F_{zL2} = mg\dfrac{a}{2L} + ma_x\dfrac{h_g}{2L} \\ F_{zR2} = mg\dfrac{a}{2L} + ma_x\dfrac{h_g}{2L} \end{cases} \tag{3}$$

Where,

$a$ = Front wheelbase

$b$ = Rear wheelbase

$L$ = Vehicle wheelbase

$B$ = Vehicle track width

$h_g$ = Height of center of gravity

$m$ = Gross vehicle weight

$g$ = Gravitational acceleration

*A. Calculated using the slip rate and adhesion coefficient*

The slip rate calculation for each wheel is shown in Formula (4):

$$s_{ij} = \frac{R\omega_{ij} - V_x}{R\omega_{ij}} \tag{4}$$

Where,

$s_{ij}$= Wheel slip ratio

$R$ = Wheel rolling radius.

$\omega_{ij}$= Rotational speed of each wheel

$V_x$= Longitudinal speed of the vehicle during travel

$ij$ = L1, R1, L2, R2

Define the utilization coefficient of adhesion for each wheel as the ratio of the wheel's vertical force to its longitudinal force, calculated using formula (5):

$$\mu_{ij} = \frac{F_{x_{ij}}}{F_{z_{ij}}} \tag{5}$$

Where,

$\mu_{ij}$= Utilization coefficient of adhesion for each wheel

$F_{x_{ij}}$= Longitudinal force acting on each wheel

$F_{z_{ij}}$= Vertical force acting on each wheel

## 3. Road Surface Recognition Controller Design

This paper employs fuzzy control to identify road surfaces using wheel slip rate and adhesion coefficient as inputs, outputting the similarity between the current road surface and various typical surfaces. A weighted method is used to estimate the optimal slip rate for each surface. Typical surfaces include: ice, snow-covered, wet cobblestone, dry gravel, wet asphalt, dry cement, and dry asphalt surfaces.

The corresponding optimal slip rates $s_{opt}$ for each pavement type are shown in Table 1.

Table 1
Key parameters of typical pavements

| **Road surface type** | **$s_{opt}$** |
|---|---|
| Icy road surface | 0.03 |
| Snow-covered road surface | 0.06 |
| Wet cobblestone pavement | 0.09 |
| Dry gravel road surface | 0.12 |
| Wet asphalt pavement | 0.13 |
| Dry cement pavement | 0.16 |
| Dry asphalt pavement | 0.17 |

During routine driving, vehicles spend the majority of time in the low slip rate range. Accurate identification of this region directly determines the performance of vehicle stability control systems under normal operating conditions. Therefore, higher recognition precision is required when slip rates are low. The slip rate is fuzzyfied into four fuzzy subsets denoted as {Very Small, Small, Medium, Large}, abbreviated as {VS, S, L, M}, as shown in Figure 2(a) for the slip rate membership function. The wheel is fuzzyfied using the adhesion coefficient to yield the adhesion coefficient membership function depicted in Figure 2(b).

The degree of road surface similarity is categorized into five specific levels ranging from “completely dissimilar” to “completely similar.” Each level is denoted by $S_i$(i=1~5), with

Table 2
Fuzzy rule table

| **Ice/Snow/Wet Pebbles/Dry Sand/Wet Asphalt/Dry Cement/Dry Asphalt** | | **s** | | | |
|---|---|---|---|---|---|
| | | **VS** | **S** | **M** | **L** |
| μ | $\mu_1$ | S5/S4/S3/S2/S2/S2/S2 | S4/S5/S4/S3/S2/S2/S2 | S3/S4/S3/S2/S2/S2/S2 | S3/S4/S3/S3/S2/S2/S2 |
| | $\mu_2$ | S4/S5/S4/S3/S3/S3/S3 | S3/S5/S5/S4/S3/S3/S3 | S2/S4/S4/S3/S3/S3/S3 | S3/S5/S4/S4/S3/S3/S3 |
| | $\mu_3$ | S3/S4/S5/S4/S4/S4/S4 | S2/S4/S5/S5/S4/S4/S4 | S2/S3/S5/S4/S4/S4/S4 | S2/S4/S5/S5/S4/S4/S4 |
| | $\mu_4$ | S2/S3/S4/S5/S5/S5/S5 | S2/S3/S5/S5/S5/S5/S5 | S2/S2/S5/S5/S5/S5/S5 | S2/S3/S5/S5/S5/S4/S4 |
| | $\mu_5$ | S2/S2/S4/S5/S5/S5/S5 | S2/S2/S4/S5/S5/S5/S5 | S2/S2/S4/S5/S5/S5/S5 | S2/S2/S4/S5/S5/S5/S5 |
| | $\mu_6$ | S1/S2/S3/S5/S5/S5/S5 | S1/S2/S3/S5/S5/S5/S5 | S1/S2/S3/S5/S5/S5/S5 | S1/S2/S3/S4/S5/S5/S5 |
| | $\mu_7$ | S1/S1/S2/S4/S5/S5/S5 | S1/S1/S2/S4/S5/S5/S5 | S1/S1/S2/S4/S5/S5/S5 | S1/S1/S2/S3/S4/S5/S5 |

the fuzzy inference rules shown in Table 2.

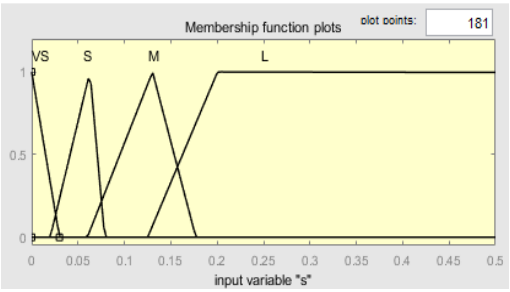


(a) Slip rate membership function

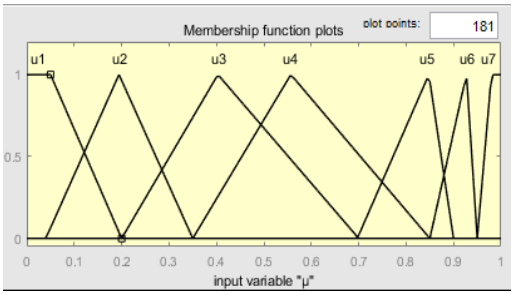


(b) Utilizing the membership function of the adhesion coefficient

Fig. 2. Input membership function

Gaussian membership functions are employed to refine fuzzy values. The similarity of road surfaces is represented by $x_1$, $x_2$, $x_3$, $x_4$, $x_5$, $x_6$ and $x_7$, with the corresponding similarity membership functions illustrated in Figure 3.

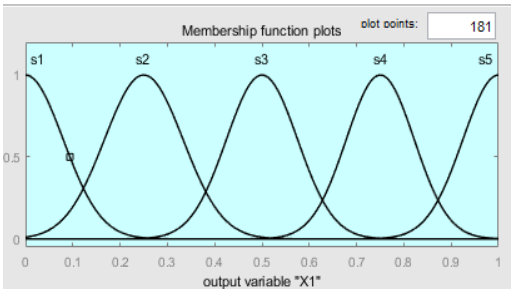


Fig. 3. Membership function of similarity

The weighted average of the output results yields the optimal slip rate for the current road surface[13], as shown in Equation (6).

$$s_{opt} = \frac{\sum_{i=1}^{7} x_i s_{opt_i}}{\sum_{i=1}^{7} x_i} \tag{6}$$

Where,

$s_{opt_i}$ = Optimal Slip Rates for Seven Typical Pavement Categories

## 4. Design of Drive Anti-Slip Controller

### *A. Design of a Standard Fuzzy PID Controller*

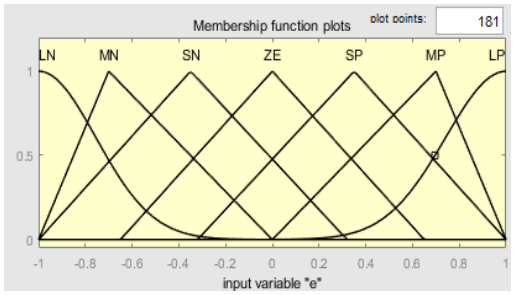


(a) Membership function of error e

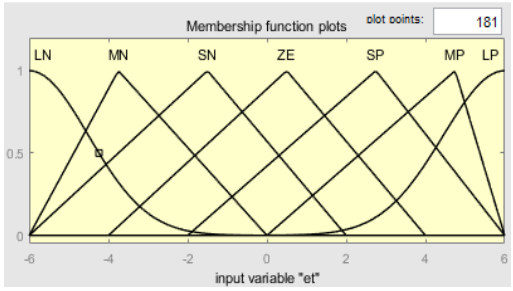


(b) Membership function of error change rate ec

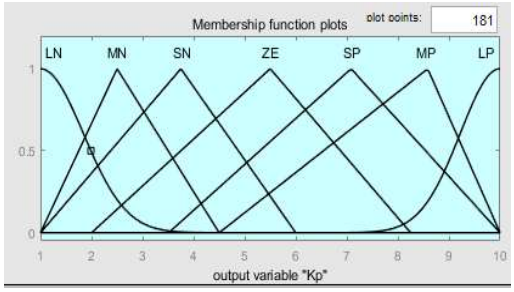


(c) Membership function of $K_p$

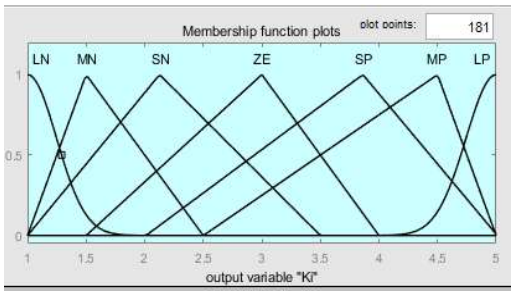


(d) Membership function of $K_i$

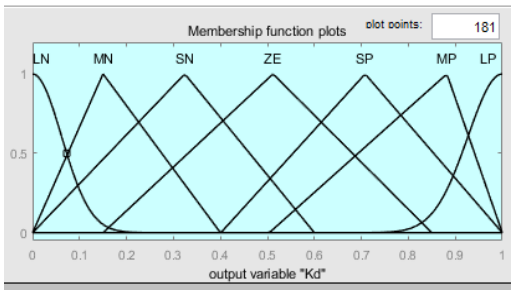


(e) Membership function of $K_d$

Fig. 4. Membership functions of fuzzy PID output variables

The deviation e and deviation rate of change ec of the slip

Table 3
Fuzzy rule table for $K_p$, $K_i$, and $K_d$ in the Fuzzy PID Controller

| $K_p/K_i/K_d$ | | ec | | | | | | |
|---|---|---|---|---|---|---|---|---|
| | | **LN** | **MN** | **SN** | **ZE** | **SP** | **MP** | **LP** |
| | LN | LP/SN/LP | LP/SN/LP | LN/SP/MP | LN/MN/MP | MP/MP/LN | LP/MN/MP | LP/MP/SN |
| | MN | LP/SN/LP | MP/SN/ZE | LN/MN/ZE | LN/MN/ZE | MP/MP/LN | LP/ZE/MP | MP/MP/ZE |
| | SN | MP/LN/MP | MP/MN/SP | LN/ZE/MN | LP/ZE/ZE | MN/LP/LN | MP/MP/MP | ZE/LP/LP |
| **e** | ZE | MP/LN/SP | MP/ZE/MN | LP/ZE/MN | MP/MP/ZE | MN/LN/LN | ZE/LP/MP | LP/LP/LP |
| | SP | SP/ZE/SP | SP/ZE/MN | MP/MP/ZE | ZE/LP/ZE | MN/LN/LP | ZE/LP/MP | MN/LN/LP |
| | MP | SP/MP/MN | SP/MP/ZE | ZE/LP/ZE | MN/LN/ZE | SP/SN/LP | MN/LN/MP | MN/SN/LP |
| | LP | MP/MP/LN | ZE/MP/MP | ZE/LP/MP | MN/LN/MP | SP/SN/SN | MN/SN/MP | SP/SN/SN |

rate are used as input variables, while the three parameters $K_p$, $K_i$, and $K_d$ of the PID controller serve as output variables. Figures 4(a) and 4(b) show the membership functions of the fuzzy controller inputs e and ec, while Figures 4(c), 4(d), and 4(e) display the membership functions of the outputs $K_p$, $K_i$, and $K_d$, respectively. The inputs e and ec, along with the outputs $K_p$, $K_i$, and $K_d$, are classified into the set {LN, MN, SN, ZE, SP, MP, LP}, where each element corresponds to one of seven fuzzy semantic levels: {negative large, negative medium, negative small, zero, positive small, positive medium, positive large}.

The fuzzy rules selected for designing the fuzzy PID controller are shown in Table 3.

### *B. Design of Fuzzy Controllers with Variable Domain*

Traditional fuzzy PID control algorithms exhibit weak adaptability and poor accuracy [14]. To address this issue, this paper employs scaling factors to achieve fuzzy domain scaling [15], thereby enabling real-time adjustment of PID controller parameters.

Let the basic domains of the fuzzy controller's input variables be $[-E, E]$ and $[-EC, EC]$, respectively, and the basic domain of the output variable be $[-U, U]$. The adjusted domains are denoted as $X_e$,$X_{ec}$ and $Y_y$, satisfying the relationship shown in Equation (7):

$$\begin{cases} X_e = [-\alpha_e E, \alpha_e E] \\ X_{ec} = [-\alpha_{ec} EC, \alpha_{ec} EC] \\ Y_y = [-\beta U, \beta U] \end{cases} \tag{7}$$

Table 4
Input variable scaling factor fuzzy rule table

| $\alpha_e/\alpha_{ec}$ | | ec | | | | | | |
|---|---|---|---|---|---|---|---|---|
| | | **LN** | **MN** | **SN** | **ZE** | **SP** | **MP** | **LP** |
| | LN | L | L | M | M | M | S | S |
| | MN | L | M | M | M | M | M | S |
| | SN | M | M | S | S | S | S | M |
| **e** | ZE | M | M | S | TS | S | M | M |
| | SP | M | M | S | S | S | M | M |
| | MP | S | M | M | M | M | M | L |
| | LP | S | S | M | M | M | L | L |

As shown in Table 4, the fuzzy rules for input variables are presented, where $\alpha_e$ and $\alpha_{ec}$ represent the scaling factors for e and ec, respectively. These scaling factors are divided into four fuzzy levels, with the fuzzy linguistic membership functions {Very Small, Small, Medium, Large} and corresponding fuzzy subsets {TS, S, M, L}

Table 5
Fuzzy rule table for output variable scaling factors

| β | | ec | | | | | | |
|---|---|---|---|---|---|---|---|---|
| | | **LN** | **MN** | **SN** | **ZE** | **SP** | **MP** | **LP** |
| e | LN | LB | L | M | M | S | S | TS |
| | MN | L | L | M | M | M | S | S |
| | SN | M | M | S | S | S | S | M |
| | ZE | M | M | S | TS | S | M | M |
| | SP | M | M | S | S | S | M | M |
| | MP | S | S | M | M | M | L | L |
| | LP | TS | S | S | M | M | L | LB |

Table 5 presents the fuzzy rules for output variables, where $\beta$ represents the scaling factor of the output variables. $\beta$ is divided into five fuzzy levels, with fuzzy linguistic terms {very small, small, medium, large, very large} and fuzzy subsets {TS, S, M, L, LB}.

The final model of the sliding-slope variable-domain fuzzy PID controller developed within the MATLAB/Simulink software (using the left front wheel as an example) is shown in Figure 5.

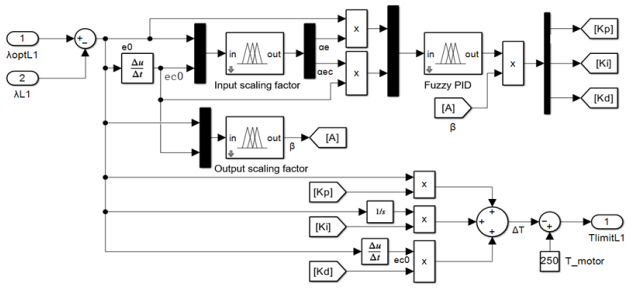


Fig. 5. Variable domain fuzzy PID-Driven Anti-Skid controller

## 5. Simulation Verification and Results Analysis

The traction control framework is shown in Figure 6. This paper uses the built-in Class B vehicle in CarSim as the controlled object.

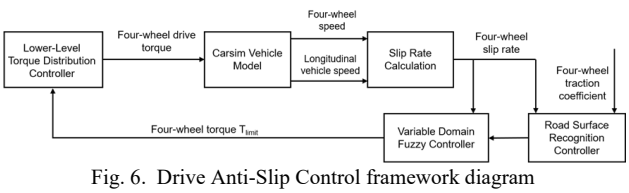


Fig. 6. Drive Anti-Slip Control framework diagram

This study employs a joint simulation platform integrating MATLAB/Simulink and CarSim to conduct acceleration tests from a standstill (target speed 100 km/h) under various typical road surface conditions. The objective is to validate the reliability and effectiveness of the designed traction control strategy.

### *A. Uniform Road Surface Traction Simulation Analysis*

Tests were conducted on a uniform snow-covered road surface with a coefficient of friction of 0.19 and an optimal slip ratio of 0.06.

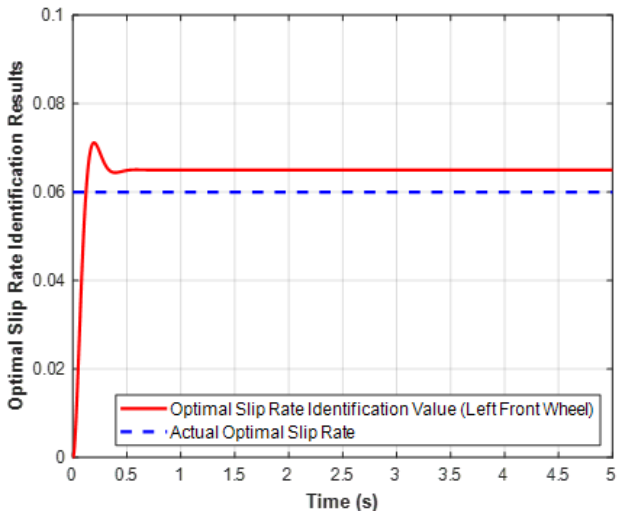


Fig. 7. Identification of optimal slip rate for uniform road surface

The optimal slip rate identification results for the left front wheel are shown in Figure 7. The road surface recognition controller can rapidly and accurately track the optimal slip rate of the road surface during the vehicle's initial acceleration phase. After a brief overshoot, the identification results quickly stabilize at a level slightly above the actual value, with an identification error of approximately 5.3%.

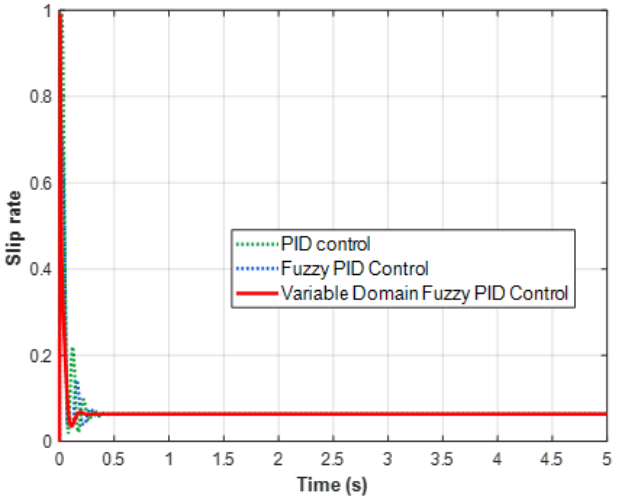


Fig. 8. Comparison of Anti-Skid Control effects for uniform road surface drive

Figure 8 shows the response results of the drive anti-slip controller. It can be observed that among the three strategies, PID control exhibits the largest overshoot and the longest settling time. Although fuzzy PID control reduces both overshoot and settling time, it still exhibits a certain degree of oscillation during the steady-state phase. In contrast, variable domain fuzzy PID control demonstrates significant advantages: it exhibits the smallest overshoot, rapidly suppresses sharp fluctuations in slip rate, and converges quickly to values near the optimal slip rate.

### *B. Simulation Analysis of Road Surface Drive Anti-Skid System*

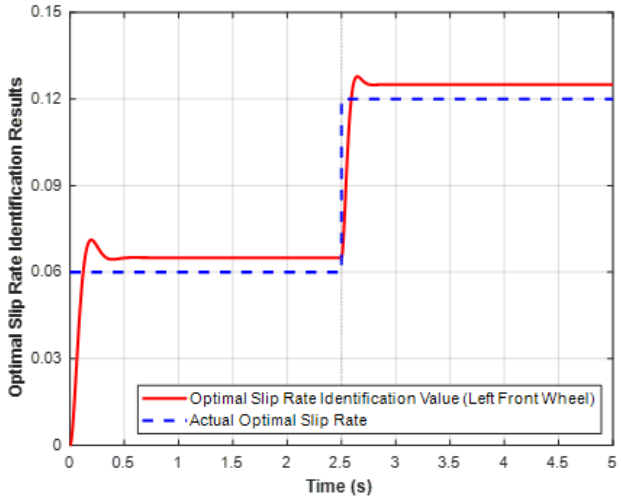


Fig. 9. Identification of optimal slip ratio for road surface alignment

Simulation tests were conducted on a snow-covered to dry sand and gravel transition road surface. The first 2.5 seconds represented a uniformly snow-covered road surface; the subsequent 2.5 seconds simulated a dry sand and gravel surface with a coefficient of adhesion of 0.61, where the optimal slip ratio was 0.12.

The optimal slip rate identification results for the left front wheel are shown in Figure 9. The identification error on snow-covered surfaces is approximately 5.3%, while the error on dry gravel surfaces is approximately 4.7%.

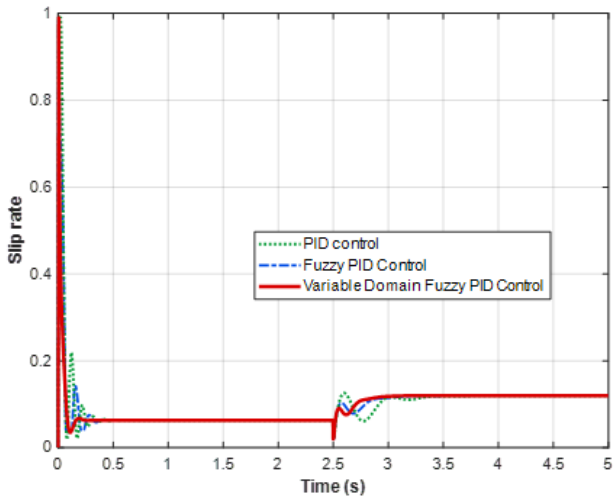


Fig. 10. Comparison of traction control performance on aligned road surfaces

As shown in Figure 10, the variable domain fuzzy PID controller demonstrates significant advantages in dynamic response on aligned road surfaces. During the initial acceleration phase, an instantaneous drive torque is applied at t=0. With zero initial vehicle speed and low road surface adhesion, wheel speed rapidly increases, causing the slip rate to

surge momentarily. The traction control system intervenes swiftly, pulling the slip rate from a near-uncontrolled state close to 1 back toward the optimal slip rate for low-adhesion surfaces, where it stabilizes. At t=2.5s, when the road surface suddenly changes, the slip rate of the left front wheel for all three controllers briefly decreases. However, the variable-domain fuzzy PID control exhibits the fastest response and the smallest oscillation amplitude. It leverages its ability to dynamically adjust the fuzzy domain to swiftly correct the control input when the error is large and rapidly converge as the system approaches the target value, thereby effectively suppressing persistent oscillations of the control input near steady-state.

### *C. Simulation Analysis of Drive-by Road Surface Skid Resistance*

Simulation testing was conducted on a split road surface consisting of snow-covered and dry gravel sections. During the simulation, the left wheels were positioned on the snow-covered surface, while the right wheels were on the dry gravel surface.

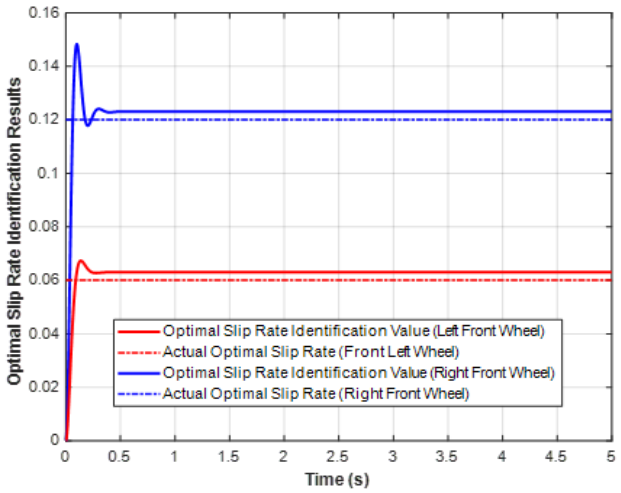


Fig. 11. Identification of optimal slip ratio for opposite road surfaces

The identification results for the optimal slip ratio of the left front wheel and right front wheel during road surface simulation are shown in Figure 11. The identification processes for the left and right front wheels exhibit distinct asymmetric dynamic characteristics. The left wheel, constrained by lower road adhesion and thus limited drive torque, exhibits a smooth, rapid, and monotonically increasing identification curve with minimal overshoot, quickly stabilizing near 0.065. The right front wheel demonstrates a rapid initial rise accompanied by significant overshoot during the start phase, with the peak slip rate briefly exceeding 0.14. This may stem from the high-grip wheel, serving as the primary driving force source, enduring abrupt changes in drive torque. Through rapid dynamic adjustments, the recognition algorithm swiftly captures the peak region of the coefficient of adhesion and ultimately converges smoothly to approximately 0.125, ensuring the wheel fully utilizes the road surface's peak grip. Both wheels' slip rate recognition values converged accurately and stably near their respective actual optimal slip rates on the road surface, validating the proposed recognition algorithm's excellent robustness and adaptive capability even under asymmetric, strongly coupled conditions.

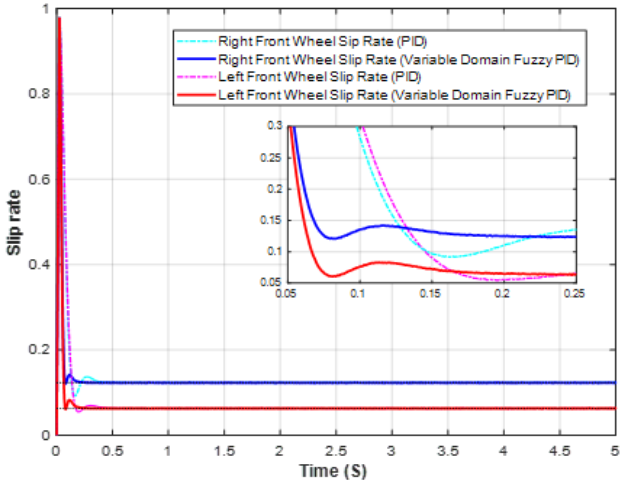


Fig. 12. Comparison of traction control performance on split road surfaces

The slip rate response curves of the vehicle on split road surfaces are shown in Figure 12. At the instant of start at t=0, both left and right wheel slip rates rapidly increase due to the step input of drive torque. Traditional PID control exhibits slow convergence during the slip rate decay phase. Particularly on the low-friction side (left front wheel), the slip rate undergoes a noticeable rebound and oscillation after reaching its trough, with prolonged adjustment time. This indicates poor adaptability under highly nonlinear, high-disturbance conditions like dual-surface roadways. The variable domain fuzzy PID controller, however, rapidly "pulls back" the slip rate to near the target value after its surge, whether on the low-traction or high-traction side. This occurs with only minor oscillations and overshoot.

## 6. Summary

To address the anti-skid requirements of distributed-drive electric vehicles under complex operating conditions, this paper proposes a composite control architecture integrating road surface condition identification with variable domain fuzzy PID control. The core of this strategy lies in two aspects: First, establishing a road surface recognition controller for optimal slip rate using a fuzzy controller driven by slip rate and utilization coefficient. Second, enhancing the fuzzy PID anti-skid controller by introducing a variable domain mechanism with adaptive scaling characteristics. Through nonlinear scaling of the domain range, this achieves online self-tuning of PID gains under varying error gradients. Finally, joint simulations under uniform, butt-jointed, and split-surface conditions demonstrate: a recognition error of 5.3% on snow-covered roads with an optimal slip rate of 0.06, and 4.7% on dry gravel roads with an optimal slip rate of 0.12. Compared to traditional PID and conventional fuzzy PID, this strategy exhibits reduced overshoot, accelerates wheel slip rate convergence to optimal values, and enhances vehicle stability during both launch and cruising.

## References


[1] F. Yi, Y. Lu, X. Zang, *et al*., "Research and analysis on the development of electric vehicles in the world," *Industry Science and Engineering*, vol. 2, no. 11, 2025.

[2] Y. Yu, L. Yang, and W. Chao, "Development and validation of AEBS anti-slip control model for in-wheel motor drive EV in AMESim co-simulation with Matlab/Simulink," *Journal of Physics: Conference Series*, vol. 2219, no. 1, Art. no. 012013, 2022.

[3] A. M. Zavatsky, A. V. Keller, S. S. Shadrin, *et al*., "Development of an electric all-wheel-drive simulation model used to test torque distribution algorithms," *Energies*, vol. 16, no. 20, Art. no. 7144, 2023.

[4] H. Fujimoto, K. Fujii, and N. Takahashi, "Vehicle stability control of electric vehicle with slip-ratio and cornering stiffness estimation," in *Proc. IEEE/ASME Int. Conf. Advanced Intelligent Mechatronics (AIM)*, Zurich, Switzerland, 2007, pp. 1–6.

[5] A. Busch, M. Wielitzka, T. Ortmaier, *et al*., "Adaptive model predictive traction control for electric vehicles," in *Proc. 18th European Control Conf. (ECC)*, 2019, pp. 1239–1244.

[6] R. Jafari, P. Sarhadi, A. Paykani, *et al*., "Integrated energy optimization and stability control using deep reinforcement learning for an all-wheel-drive electric vehicle," *IEEE Open Journal of Vehicular Technology*, 2025.

[7] T. Ueno, B.-M. Nguyen, and H. Fujimoto, "Driving force control for in-wheel motor electric vehicles with wheel speed limiter and absolute stability analysis," in *Proc. IECON 2023 – 49th Annual Conf. IEEE Industrial Electronics Society*, Singapore, 2023, pp. 1–6.

[8] N. T. Nguyen, M. C. Ta, T. Vo-Duy, and V. Ivanov, "Enhanced fuzzy-MFC-based traction control system for electric vehicles," in *Proc. IEEE Vehicle Power and Propulsion Conf. (VPPC)*, Milan, Italy, 2023, pp. 1–6.

[9] L. Q. Jin, M. Ling, and W. Yue, "Tire-road friction estimation and traction control strategy for motorized electric vehicle," *PLOS One*, vol. 12, no. 6, Art. no. e0179526, 2017.

[10] X. Gao and C. Lin, "Electromechanical coupling approach for traction control system of distributed drive electric vehicles," in *E3S Web of Conferences*, vol. 236, Art. no. 01007, 2021.

[11] B. Leng, L. Xiong, Z. Yu, *et al*., "Robust variable structure anti-slip control method of a distributed drive electric vehicle," *IEEE Access*, vol. 8, pp. 162196–162208, 2020.

[12] Z. Yu, R. Zhang, X. Lu, *et al*., "Robust adaptive anti-slip regulation controller for a distributed-drive electric vehicle considering the driver's intended driving torque," *Proc. Inst. Mech. Eng., Part D: J. Automobile Engineering*, vol. 232, no. 4, pp. 562–576, 2018.

[13] J. S. Qiang, "Anti-slip control research for the electric vehicle of in-wheel motor drive," *E3S Web of Conferences*, vol. 53, Art. no. 01017, 2018.

[14] K. Sun, J. Xu, and S. Zheng, "Analysis and design of wire winding tension control system based on genetic algorithm and fuzzy PID," *Trans. Inst. Meas. Control*, vol. 47, no. 16, pp. 3203–3212, 2025.

[15] V. A. Klimov, V. A. Antonyan, V. A. Keller, *et al*., "Anti-slip control system with self-oscillation suppression function for the electromechanical drive of wheeled vehicles," *World Electric Vehicle Journal*, vol. 16, no. 2, p. 84, 2025.